▌ Supramolecular Chemistry

Controlling the Surface Functionalization of Ultrasmall Gold Nanoparticles by Sequence-Defined Macromolecules

Selina Beatrice van der Meer,[a] Theresa Seiler,[b] Christin Buchmann,[b] Georgia Partalidou,[b] Sophia Boden,[b] Kateryna Loza,[a] Marc Heggen,[c] Jürgen Linders,[d] Oleg Prymak,[a] Cristiano L. P. Oliveira,[e] Laura Hartmann,*[b] and Matthias Epple*[a]

Abstract: Ultrasmall gold nanoparticles (diameter about 2 nm) were surface-functionalized with cysteine-carrying precision macromolecules. These consisted of sequence-defined oligo(amidoamine)s (OAAs) with either two or six cysteine molecules for binding to the gold surface and either with or without a PEG chain (3400 Da). They were characterized by ^{1}H NMR spectroscopy, ^{1}H NMR diffusion-ordered spectroscopy (DOSY), small-angle X-ray scattering (SAXS), and high-resolution transmission electron microscopy. The number of precision macromolecules per nanoparticle was determined after fluorescent labeling by UV spectroscopy and also by quantitative ^{1}H NMR spectroscopy. Each nanoparticle carried between 40 and 100 OAA ligands, depending on the number of cysteine units per OAA. The footprint of each ligand was about 0.074 nm^2 per cysteine molecule. OAAs are well suited to stabilize ultrasmall gold nanoparticles by selective surface conjugation and can be used to selectively cover their surface. The presence of the PEG chain considerably increased the hydrodynamic diameter of both dissolved macromolecules and macromolecule-conjugated gold nanoparticles.

Introduction

Peptide-mimetic oligo(amidoamine)s (OAAs) represent a new ligand class for the surface functionalization of gold nanoparticles. Similar to the peptide solid-phase synthesis according to

[a] Dr. S. B. van der Meer, Dr. K. Loza, Dr. O. Prymak, Prof. Dr. M. Epple
Inorganic Chemistry and Center for Nanointegration Duisburg-Essen (CeNIDE), University of Duisburg-Essen
Universitätsstr. 5–7, 45117 Essen (Germany)
E-mail: matthias.epple@uni-due.de

[b] T. Seiler, C. Buchmann, G. Partalidou, Dr. S. Boden, Prof. Dr. L. Hartmann
Organic Chemistry and Macromolecular Chemistry
Heinrich Heine-University Düsseldorf, Universitätsstr. 1
40225 Düsseldorf (Germany)
E-mail: laura.hartmann@hhu.de

[c] Dr. M. Heggen
Ernst Ruska-Center for Microscopy and Spectroscopy with Electrons
Forschungszentrum Jülich GmbH, 52425 Jülich (Germany)

[d] Dr. J. Linders
Physical Chemistry and Center for Nanointegration Duisburg-Essen (CeNIDE), University of Duisburg-Essen, Universitätsstr. 5–7
45117 Essen (Germany)

[e] Prof. Dr. C. L. P. Oliveira
Institute of Physics, University of São Paulo
Rua do Matão 1371, São Paulo, São Paulo, 05508-090 (Brazil)

🖳 Supporting information and the ORCID identification number(s) for the author(s) of this article can be found under:
https://doi.org/10.1002/chem.202003804.

Merrifield,[1] OAAs are synthesized via stepwise addition of building blocks on a solid support, giving access to monodisperse, sequence-defined macromolecules. In addition to readily available amino acids, we have developed a library of non-natural building blocks allowing the introduction of different functional units within the main or the side chain of the resulting macromolecule.[2] Earlier, we have reported the synthesis of glycosylated OAAs and their potential to mimic natural glycans and their interaction with carbohydrate-recognizing receptors such as lectins or bacterial adhesins.[3] The attachment of glycosylated OAAs to gold nanoparticles via a terminal thiol group allowed for a straightforward read-out of lectin binding by UV spectroscopy, based on the surface plasmon resonance effects of the gold nanoparticles.[4] However, the degree of functionalization of the gold nanoparticles is variable for OAAs of different composition and structure, for example, when going from one to three carbohydrate residues per OAA. In order to understand structure-property correlations of OAA-functionalized gold nanoparticles, a control over the degree of functionalization (or surface coverage) is required.

To elucidate the effect of multi-thiol ligands on the degree of functionalization of gold nanoparticles in detail, we have used ultrasmall gold nanoparticles of about 2 nm diameter.[5] The term "ultrasmall gold nanoparticles" has been coined to distinguish such particles from "classical" larger gold nanoparticles (10–15 nm), prepared for example, by the Turkevich method.[6] They are typically a bit larger than atom-sharp gold clusters (1 to 2 nm) and have a diameter between 1 and 3 nm, although there is no strict size range for them which is generally accepted.[7] The fact that NMR spectroscopy is possible

Chemistry–A European Journal

Full Paper
doi.org/10.1002/chem.202003804

Chemistry Europe
European Chemical
Societies Publishing

with such ultrasmall nanoparticles is advantageous for a quantitative assessment of their surface composition, especially to determine the number of ligands and thus the degree of surface functionalization.[5b, c, 8]

Here we demonstrate how peptide-mimetic OAAs can be used as tailor-made surface coating ligands for ultrasmall gold nanoparticles. The length and number of sulfur binding atoms of the OAAs was systematically varied to assess the nature of their interaction with the gold nanoparticles, like molecular footprint and the possibility to cover the particle surface. This was elucidated by colloid-chemical methods and extensive NMR spectroscopic investigations.

Experimental Section

Chemicals

A solution of tetrachloroauric acid (HAuCl$_4$) was prepared by dissolving elemental gold ($\geq$99%) in *aqua regia*. Ultrapure water (Purelab ultra instrument from ELGA) was used for all nanoparticle syntheses and purifications unless otherwise noted. Before all reactions involving nanoparticles, all glassware was cleaned with boiling *aqua regia* and thoroughly washed with ultrapure water afterwards.

Sodium borohydride (NaBH$_4$, $\geq$96%), deuterium oxide (D$_2$O, 99%), diethyl ether (with BHT as inhibitor, 99.8%), triisopropylsilane (98%; TIPS), 2,2′-(ethylenedioxy)bis(ethylamine) (98%), ethyl trifluoroacetate (99%), and succinic anhydride (>99%) were obtained from Sigma–Aldrich. Trityl chloride (98%) and piperidine (99%), were obtained from Acros Organics. PyBOP (benzotriazole-1-yl-oxy-tris-pyrrolidino-phosphonium hexafluorophosphate) and Fmoc-L-Cys(Trt)-OH was obtained from Iris Biotech. 9-Fluorenylmethyl chloroformate (Fmoc-Cl, 98%) was purchased from Chempur. N,N-Diisopropylethylamine (99%; DIPEA) was obtained from Carl Roth. Trifluoroacetic acid (99%; TFA) was obtained from Fluorochem. Dichloromethane (99.99%; DCM), sodium chloride (99.98%), tetrahydrofuran (THF) (analytical reagent grade), ethyl acetate (analytical reagent grade), sodium hydrogen carbonate (analytical reagent grade), toluene (analytical reagent grade), were obtained from Fisher Scientific. Tentagel® S RAM (Rink Amide) resin (Capacity 0.23 mmol g^{-1}) and Tentagel® Pap (Capacity 0.16 mmol g^{-1}) were obtained from Rapp Polymere. Fluorescein isothiocyanate isomer I was obtained from J&K Scientific. Peptide synthesis-grade N,N-dimethylformamide was used. All solvents were of p.a. reagent grade, and all solvents and reagents were used without further purification.

Synthesis of oligo(amidoamine)s (OAAs)

OAAs were prepared according to previously established protocols.[9] As building blocks, commercially available amino acid cysteine (Cys) and the tailor-made building block EDS[10] introducing an ethylene glycol spacer in the main chain were assembled following standard Fmoc-coupling protocols. In total, four different OAAs were synthesized presenting either two or six cysteines. As additional chain promoting the colloidal stabilization of the gold nanoparticles, either a short chain consisting of three EDS building blocks or a long PEG chain of 3400 Da were used. The PEG unit was incorporated with a preloaded Tentagel® Rink Amid resin. The OAAs were also synthesized as fluorescein-labeled compounds for analysis by UV spectroscopy (determination of the number of OAAs per gold nanoparticle).

The building block EDS was synthesized according to previously reported protocol with an overall yield of 54%.[10] All solid phase reactions were performed in polypropylene reactors with a polyethylene frit closed at the bottom with a luer stopper. The batch sizes for synthesizing the oligomers using solid phase synthesis varied between 0.05 and 0.2 mmol. Tentagel® S Ram resin with a loading of 0.23 mmol g^{-1} and Tentagel® Pap with a loading of 0.16 mmol g^{-1} were used for PEG-attached oligo(amidoamine)s.

Precise oligomers were synthesized on solid support by coupling and Fmoc deprotection protocols. For preparation the resin was swelled twice for 15 min in DCM. Afterwards the resin was washed five times with DMF. For cleavage of the Fmoc group of the resin as well as for the coupled building blocks or amino acids, the resin was treated with a solution of 25 vol% piperidine in DMF. The deprotection time was 2×15 min. After the deprotection, the resin was washed ten times with DMF. A building block or amino acid (5 equiv.) and the coupling reagent PyBOP (5 equiv.) were dissolved in DMF. Afterwards DIPEA (10 equiv.) was added and the solution was flushed with nitrogen for 1 min. The solution was subsequently added to the previous deprotected resin and the reaction was shaken for 1 h at room temperature. The resin was then washed 10 times with DMF. For attachment of a fluorophore, each resin of an oligo(amidoamine) batch was divided into two halves, one half of which was then functionalized with a fluorophore.

The fluorophore FITC-isothiocyanate (1.1 equiv.) was dissolved in 6 mL DMF before DIPEA (10 equiv.) was added, and the solution was flushed with nitrogen for 1 min. Then the mixture was subsequently added to the resin and shaken for 18 h. An excess of reagents was removed by washing. For double coupling, the procedure was repeated the same way once more. Afterwards the resin was washed 10 times alternatingly with DMF, DCM and MeOH.

For microcleavage, a small amount of resin was treated with a solution of 95 vol% TFA, 2.5 vol% TIPS, and 2.5 vol% DCM for 20 min. For precipitation of the product, the cleavage solution was filtered and added to cold diethyl ether. The suspension was centrifuged, and the supernatant was decanted. The remaining residue was dried under nitrogen, dissolved in 0.5 mL of water or water and acetonitrile and measured by HPLC. For macrocleavage, the resin was washed 10 times with 8 mL DCM before the cleavage solution was added. The cleavage solution for the Tentagel® S Ram resin consisted of a mixture of TFA/TIPS/DCM. Depending on the number of cysteine units of the oligomer, the concentrations of TFA and TIPS varied from 85 to 95 vol% and from 5 to 15 vol%, respectively. The cleavage solution for the Tentagel® Pap resin consisted of a mixture of TFA/TIPS/thioanisol. The concentration of thioanisol was always 5 vol%, the concentration of TIPS varied between 5 and 15 vol%, and the concentration of TFA varied between 85 and 95 vol% depending on the number of cysteine units of the oligomer. After the reaction was shaken for 1 h, the filtrated was added dropwise to cold diethyl ether. The resin was washed with an additional aliquot of the cleaving solution and DCM which were then also added to the cooled ether. The ether phase was centrifuged, and the supernatant was decanted off. The remaining residue was dried under nitrogen, dissolved in 6 mL of water and lyophilized.

For further details on OAA synthesis and characterization, see the Supporting Information.

Nanoparticle synthesis

The ultrasmall gold nanoparticles were prepared by a modified one-phase Brust synthesis,[11] following the synthetic protocols reported earlier.[5a–d] The cysteine-terminated OAAs (short-/long-2,

3.75 μmol, or short-/long-6, 1.25 μmol) were dissolved in 10 mL ultrapure water, respectively. The pH was adjusted to 7 by addition of 0.1 M sodium hydroxide solution under continuous stirring. The solution was degassed with argon, and 50 μL of 50 mM tetrachloroauric acid (2.5 μmol) were added. After the yellow color of the tetrachloroauric acid had vanished, 50 μL of a 200 mM ice-cold aqueous sodium borohydride solution (10 μmol) were added. After the addition of sodium borohydride, the solution rapidly turned light-brown, and the dispersion was stirred for one hour at room temperature. The by-products were removed from the dispersion by ultrafiltration with centrifuge filters (3 kDa molecular weight cut-off; Amicon®; Merck). The dispersion was centrifuged for 30 min at 4000 rpm. The functionalized ultrasmall gold nanoparticle were deposited as brown dispersion in the lower part of the centrifuge tube. The filter was rinsed up to six times with ultrapure water. The concentrated dispersion of gold nanoparticles (≈ 300 μL) was finally extracted from the filter with a pipette.

Analytical methods

The gold concentration in the nanoparticle dispersion was determined by atomic absorption spectroscopy (AAS) with a Thermo Electron M-Series spectrometer (graphite tube furnace according to DIN EN ISO/IEC 17025:2005) after dissolving the nanoparticles in *aqua regia*.

Ultraviolet–visible spectroscopy (UV/Vis) was performed with a Varian Cary 300 instrument from 200 to 800 nm after background solvent correction (water). Suprasil® quartz glass cuvettes with a sample volume of 600 μL were used.

High-resolution imaging was performed with an aberration-corrected FEI Titan transmission electron microscope equipped with a Cs-probe corrector (CEOS Company) operating at 300 kV.[12]

The nanoparticle sample was dispersed in 600 μL D_2O for NMR spectroscopy. ^1H NMR spectra were recorded with a Bruker-Avance III 600 MHz spectrometer at room temperature. ^1H DOSY (diffusion ordered spectroscopy) experiments were performed in non-spinning mode at 25 °C on a Bruker-Avance 500 MHz spectrometer. The spectra were Fourier-transformed, phased and integrated in the program TopSpin. Plotting and fitting of the linearized diffusion data according to the Stejskal–Tanner equation[13] were performed with Origin Pro2017 [Eq. (1)]:

$$\ln\left(\frac{I}{I_0}\right) = -\gamma^2 \delta^2 \left(\Delta - \frac{\delta}{3}\right) \cdot D \cdot G^2 \qquad (1)$$

with I the signal intensity, I_0 the signal intensity without gradient, γ the gyromagnetic ratio of ^1H (26.752×10^7 rad$T^{-1}s^{-1}$), δ the diffusion gradient pulse length (0.001 s), Δ the diffusion delay (0.03 s), G the gradient strength, and D the translational diffusion coefficient.

The Stejskal–Tanner plots of all nanoparticle signals were first analyzed separately. Upon yielding the same diffusion coefficient within the error margin, the relative intensities I/I_0 for all signals were averaged. Error bars for the averaged data points represent the standard deviation. The accuracy of the diffusion coefficient was determined by averaging the errors obtained from the 2D-DOSY spectrum.

The hydrodynamic diameter was then calculated by the Stokes–Einstein equation [Eq. (2)]:

$$d_H = \frac{k \cdot T}{3\pi \cdot \eta \cdot D} \qquad (2)$$

with d_H the hydrodynamic diameter, k the Boltzmann constant (1.380649×10^{-23} JK^{-1}), T the temperature in K (298.15), η the dynamic viscosity of D_2O at 25 °C (1.0963 MPa s^{-1}), and D the translational diffusion coefficient from Equation (1).

SAXS measurements were performed at the Brazilian Synchrotron Light Laboratory at the SAXS1 beamline[14] under project number ID 20180110. The samples were measured in solution using a sample holder[15] sealed with two mica windows and Teflon seals, allowing the cell to be placed in vacuum. The sample width was 1 mm. The sample holder was coupled to a water-circulating thermal bath, allowing measurements at controlled temperature. The radiation wavelength was $\lambda = 0.148$ nm, and the sample to detector distance was 3,030 mm. A rectangular beam with dimensions 300×100 μm^2 was used. The 2D scattering data was collected on a Dectris PilatusTM 300k detector, and the integration of the SAXS patterns and data treatment were carried out with the FIT2D software.[16] Pure water was used for blank scattering subtraction. Error estimation and normalization to an absolute scale were performed with a self-written software. The obtained 1D curves give the scattering intensity as a function of the reciprocal space momentum transfer modulus $q = 4\pi(\sin\theta)/\lambda$ and 2θ the scattering angle. The experimental setup provided a q range of 0.06 to 1.5 nm^{-1}. However, due to the low concentration and small size of the nanoparticles, some initial points of the treated SAXS curves were not useful and had to be discarded. The scattering intensities for the nanoparticles were modeled assuming a polydisperse system of spheres with a Shulz–Zimm distribution for the particle size with the presence of aggregates.[17] From the data analysis, the average radius of the nanoparticles, their polydispersity and the overall radius of gyration of the aggregates were retrieved.

^1H NMR spectra (300 MHz and 600 MHz) of OAAs were recorded on a Bruker Avance III 600 or a Bruker Avance III 300 at room temperature. As internal standard the signal of non-deuterated solvent was used, that is, for ^1H NMR $\delta = 4.79$ ppm for D_2O and $\delta = 2.84$ ppm for [D_6]acetone.

HPLC measurements were performed on an Agilent 1260 Infinity instrument, which was coupled to a variable wavelength detector (VWD) (set to 214 nm) and a 6120 quadrupole mass spectrometer containing an electrospray ionization (ESI) source (operated in positive ionization mode in a m/z range of 200 to 2000 Da). As HPLC column, a RP Column (Poroshell 120 EC-C18, 3.0·50 mm, 2.5 μm) from MZ Analysetechnik was used. The mobile phases A (H_2O/MeCN; 95/5) and B (H_2O/MeCN; 5/95) contained 0.1% of formic acid. The temperature was set to 25 °C, and the flow rate was set to 0.4 mL min^{-1}. UV and MS analysis were done within the Open-Lab ChemStation software for LC/MS from Agilent Technologies. Purities of the compounds were determined by the integrations of the signals given at an absorption at 214 nm.

High resolution ESI (HR-ESI) measurements were performed on a Bruker UHR-QTOF maXis 4G instrument (Bruker Daltonics) with a direct inlet via syringe pump, an ESI source and a quadrupole followed by a time-of-flight (QTOF) mass analyzer.

OAAs were analyzed with a Bruker MALDI-TOF Ultraflex I (Bruker Daltonics) system with 2,5-dihydroxybenzoic acid (DHB) and α-cyano-4-hydroxycinnamic acid (CHCA) as matrix. The ratio of matrix to compound was 10:1. The spectra were acquired in both linear (m/z range 1000–4000 D) and reflector mode (m/z range 2000–20 000 Da). The reflector mode was calibrated with a protein mixture whereas the linear mode was not calibrated.

Gel permeation chromatography (GPC) was performed with an Agilent 1200 series HPLC system equipped with three aqueous GPC columns from Polymer Standards Service (PSS; Mainz, Germany;

Chemistry–A European Journal

Full Paper
doi.org/10.1002/chem.202003804

Chemistry Europe
European Chemical
Societies Publishing

Suprema Lux analytical 8 mm diameter, 5 μm particle size, precolumn of 50 mm, 2×100 Å of 300 mm, 1000 Å of 300 mm). The GPC eluent consisted of MilliQ water with 50 mM NaH_2PO_4, 150 mM NaCl, 250 ppm NaN_3, of pH 7 + 30% acetonitrile, filtered through an inline 0.1 μm membrane filter. The flow rate was 1 mL min^{-1}. UV spectra were recorded on a Waters 486 Tunable Absorbance Detector. Multi-angle light scattering- and differential refractive index spectra were recorded using miniDAWN TREOS and Optilab rEX instruments, respectively, both from Wyatt Technologies EU. Data analysis was performed with the Astra 5 software using a *dn/dc* value of 0.156 mL g^{-1} for all oligo(amidoamine)s.

Final lyophilization of the oligo(amidoamine)s was performed with an Alpha 1–4 LD plus instrument from Marin Christ Freeze Dryers GmbH (Osterode, Germany) at −54 °C and 0.1 mbar.

Results and Discussion

OAAs were prepared according to previously established protocols[9] with the amino acid cysteine (Cys) and the tailor-made building block EDS (ethylene glycol diamine succinic acid),[10] introducing an ethylene glycol spacer in the main chain. Four different OAAs were synthesized containing either two or six cysteines, each carrying a thiol unit. The surface of the ultrasmall gold nanoparticles (metallic core: 2 nm) was covered with these functional ligands. As additional chain promoting the colloidal stabilization of the gold nanoparticles, either a short chain consisting of three EDS building blocks (EDS$_3$) or a long chain consisting of a PEG (average molecular weight:

3,400 Da) was incorporated. Figure 1 shows the whole set of synthesized OAAs.

The cysteine units represent the surface-binding part of the OAAs to the gold nanoparticles due to their aurophilicity. Our aim was to elucidate the relationship between the number of thiol groups and the degree of functionalization, that is, the number of OAAs per nanoparticle. The binding is assumed to be strong due to multiple binding sites per macromolecule (similar to the chelate effect), but in principle, a cross-linking of nanoparticles could also happen. Taken to the extreme, one long-chain OAA ligand with a sufficient number of thiol groups would be sufficient to completely coat a nanoparticle (Figure 2). The conjugation of the dye fluorescein isothiocyanate (FITC) to the N-terminus of the OAA allowed the quantification of number of bound OAAs on each ultrasmall gold nanoparticle, giving the surface coverage and the ligand footprint. The distance between the dye and the gold binding sites should be high enough not to influence the number of bound OAAs ligand on the gold nanoparticles.

While our main focus was on the effect of the thiol-containing segment of the ligands coating gold nanoparticles, we also varied the non-binding hydrophilic segment. We chose a large, hydrophilic segment, that is, a PEG chain of 3,400 Da ("long"), and a smaller oligoamide-based segment of three EDS building blocks (EDS$_3$; "short"). Rahme et al. have shown that increasing the molecular weight of PEG chains for coating gold nanoparticles leads to a decreasing degree of functionalization.[18] Thus
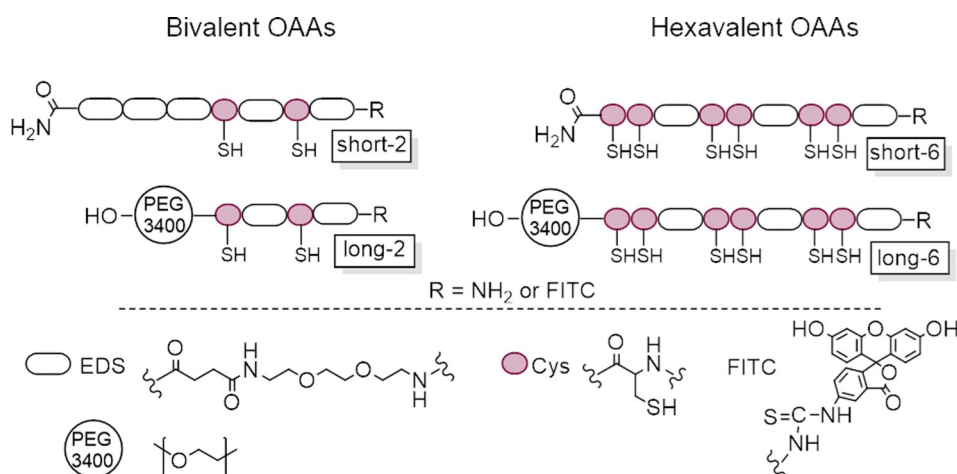

Figure 1. OAAs with two (left) and six (right) cysteine units for the surface-functionalization of ultrasmall gold nanoparticles. The sequence of the OAAs is given from C- to N-terminus (left to right), with abbreviated names referring to the length of the stabilizing chain ("short" for EDS$_3$ and "long" for PEG) and the number of thiol units per OAA (either "2" or "6"). For FITC-labeled OAAs, an "-F" is added.
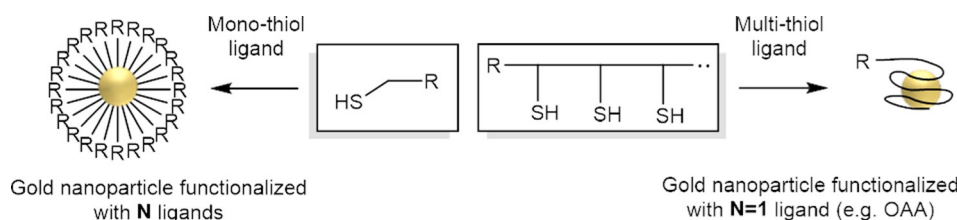

Figure 2. Concept of multivalent OAAs for the functionalization of ultrasmall gold nanoparticles (right) compared to mono-thiol ligands (left). In principle, a multivalent OAA ligand with N binding atoms should be able to fully cover one nanoparticle.

Chemistry–A European Journal

Full Paper
doi.org/10.1002/chem.202003804

Chemistry Europe
European Chemical
Societies Publishing

while keeping the thiol-containing segment constant, we expect the PEG-containing OAAs to result in a lower degree of functionalization due to steric requirements. Since the EDS$_3$ segment can also undergo intra- and intermolecular hydrogen bonding based on the amide groups within the backbone, an even denser packing and thus higher degree of functionalization is expected for the "short" OAAs. The comparison of PEG- and EDS$_3$-OAAs gives insight into the effective combination of multiple thiol-containing segments and non-binding segments to fine-tune the number of ligands on the gold nanoparticle surface.

The ultrasmall gold nanoparticles were conjugated with OAAs during the nanoparticle synthesis as described previously for peptide-coated ultrasmall gold nanoparticles,[5d] in contrast to ligand exchange as reported previously for larger gold nanoparticles.[4] The nature of the ligand-particle binding was probed by solution ^{1}H NMR spectroscopy.

Figure 3 shows representative ^{1}H NMR spectra of dissolved short-2 and of nanoparticle-conjugated short-2. There was a considerable broadening of the [1]H-resonances after binding of short-2 to the nanoparticle surface due to longer relaxation times and the presence of the metallic core.[5b, c, 8a, b] Another peculiarity was the disappearance of the peaks of the cysteine building blocks after binding to the particle surface due to the vicinity to the metal surface. As this occurred for all cysteine groups, we can safely assume that the OAA binds to the nanoparticle surface with both cysteine groups, that is, there are no dangling cysteine groups (which would result in narrower NMR peaks). The strong broadening of the ^{1}H resonances in the direct surroundings of thiol groups of R-SH ligands was also reported by Salassa et al. and used to confirm the binding to the nanoparticle surface.[5i]

The ^{1}H DOSY spectrum confirmed the attachment of short-2 to the gold nanoparticle (Figure 4). The hydrodynamic diameter more than doubled compared to the dissolved short-2, that is, from 1.93 to 4.34 nm. Note that the hydrodynamic diameter of a ligand-conjugated gold nanoparticle is not directly the sum of the diameters of the pure gold core and the free ligand because the hydration state of the free ligand is different from that of the conjugated ligand. This was also reported by Hussain et al. for 2 nm gold particles with a hydrodynamic diameter of 2.6 nm where a 5.5 kDa polymer increased the particle diameter by about 21%.[19]

Figure 5 shows the [1]H-DOSY spectra of dissolved long-2 and of nanoparticle-conjugated Au-long-2. As expected, the dissolved molecule OAA long-2 and also the Au-long-2 nanoparticles have a higher hydrodynamic diameter due to the expanded PEG chains, compared to short-2 and Au-short-2.

An HRTEM image of Au-short-2 gold nanoparticles is shown in Figure 6. The core diameter of the particles was (2.09 ± 0.30) nm.

In general, the high hydrodynamic radius led to a decrease of the effective density of all OAA-conjugated nanoparticles that prevented their analysis by disc centrifugal sedimentation (DCS), that is, no sedimentation occurred within reasonable time (12 h). Dynamic light scattering (DLS) was also not applicable because the gold core was too small for sufficient light scattering.

Scattering experiments provided further structural information on the dispersed nanoparticles. In small-angle X-ray scattering (SAXS), a monochromatic X-ray beam targets the nanoparticle dispersion and part of the radiation is scattered by interactions with the sample. Based on the scattering behavior of the sample, structural information about the nanoparticles
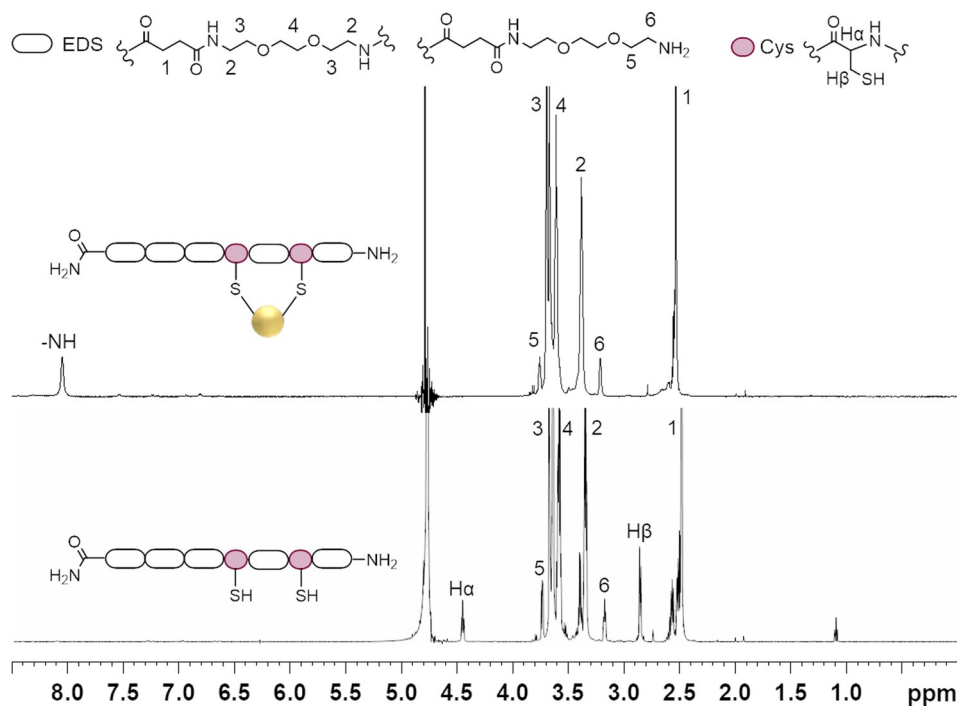

Figure 3. Structure and ^{1}H NMR spectra (600 MHz, D$_2$O) of the dissolved OAA ligand short-2 (bottom) and of short-2-conjugated ultrasmall gold nanoparticles (Au-short-2) (top). The ^{1}H NMR spectrum of long-2 is given in the Supplementary Information.
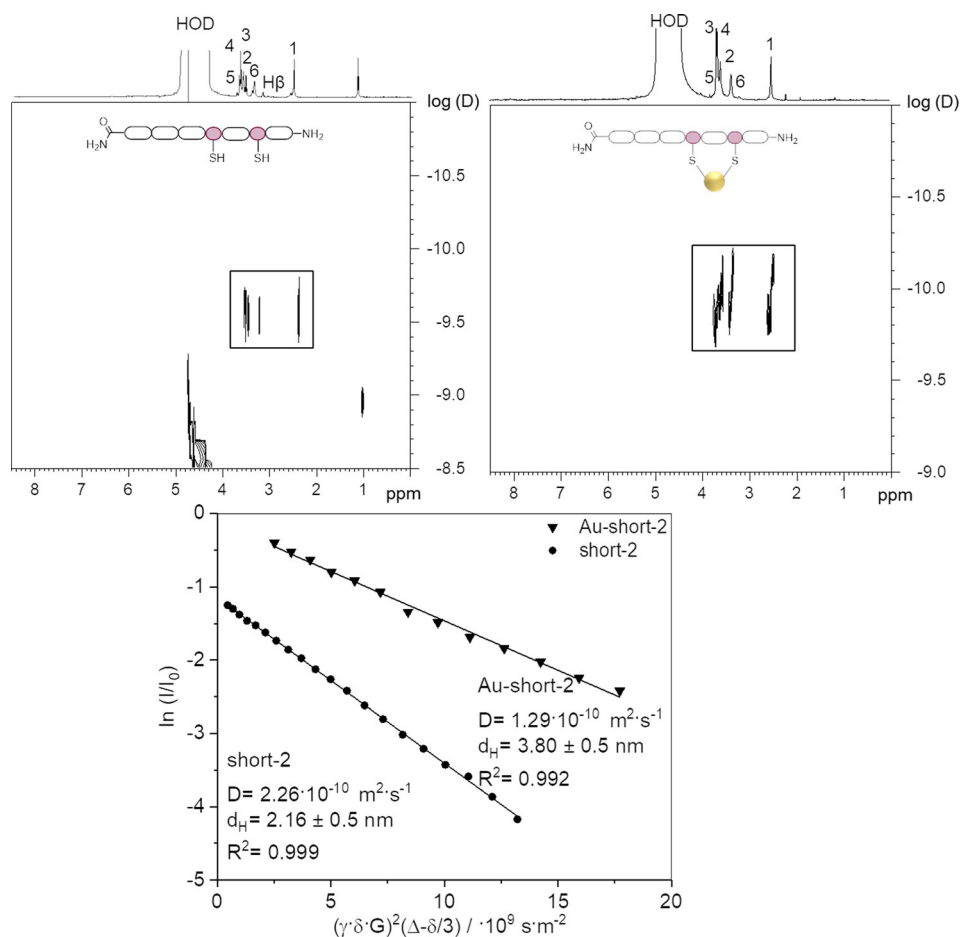
Chemistry–A European Journal

Full Paper
doi.org/10.1002/chem.202003804

Chemistry Europe
European Chemical
Societies Publishing

Figure 4. ^{1}H DOSY NMR spectrum (500 MHz, 10% D_2O) of the OAA ligand short-2 (top left) and corresponding Stejskal–Tanner plot (bottom). ^{1}H DOSY NMR spectrum (500 MHz, D_2O) spectrum of Au-short-2 (top right) and corresponding Stejskal–Tanner plot (bottom). The ligand short-2 has a signal at ≈1 ppm that moves faster than the signals from the polymer, which is due to an unknown impurity from synthesis. However, this was removed after gold conjugation of short-2 and subsequent purification (see Figure 3).

in the dispersion can be obtained, for example, average shape and size of the particles, the degree of polydispersity of the sample, and particle–particle interactions.[20] The short wavelengths of the X-rays, combined with the high electron density contrast of gold based nanoparticles dispersed in aqueous solutions, makes SAXS an ideal technique to investigate dispersed ultrasmall gold nanoparticles. Note that only the electron-rich gold core is probed, not the hydrated ligand shell. SAXS also sheds light on a possible agglomeration or on ligand-induced bridging of the nanoparticles.

The SAXS results of Au-short-2 nanoparticles are shown in Figure 7. After model fitting, the particle size distribution was obtained. A comparison of the mean diameters of the particle population analyzed by HRTEM and SAXS shows that both methods give very similar results. The SAXS result reflects a mean value from a significantly larger number of particles, that is, it gives a better representation of the size distribution of the sample than the HRTEM data. Furthermore, it probes the dispersed nanoparticles and not the dried nanoparticles.[21] From the model fitting, gold nanoparticles with a diameter of (2.0 ± 0.2) nm were obtained with a polydispersity of (0.2 ± 0.1) nm. A low number of agglomerates with an average radius

of gyration of (5 ± 1) nm (diameter (10 ± 2) nm) was also detected by SAXS analysis and may correspond to unspecific aggregates.

The attachment of a PEG chain should increase the footprint of the ligand and also the hydrophilicity of the functionalized nanoparticle. Figure 8 shows the ^{1}H NMR spectrum of dissolved OAA long-6 and of Au-long-6 nanoparticles. As with short-2, a broadening of the ^{1}H peaks after binding to the nanoparticle surface was observed due to longer relaxation times. This confirms that long-6 also binds to the nanoparticle surface with all six available cysteine groups.

The ^{1}H DOSY spectra of dissolved OAA short-6 and of nanoparticle-conjugated Au-short-6 are shown in Figure 9. The hydrodynamic diameter of dissolved short-6 was (2.75 ± 0.5) nm. For the conjugated nanoparticles Au-short-6, we measured (4.88 ± 0.5) nm. This is very similar to the OAA short-2 and the nanoparticles Au-short-2, as expected for the size of the OAA ligand.

The ^{1}H DOSY spectra for OAA long-6 and for Au-long-6 are shown in Figure 10. The diffusion coefficient of the ligand led to a hydrodynamic diameter of dissolved long-6 of 5.35 nm. The ^{1}H DOSY NMR spectrum of Au-long-6 nanoparticles
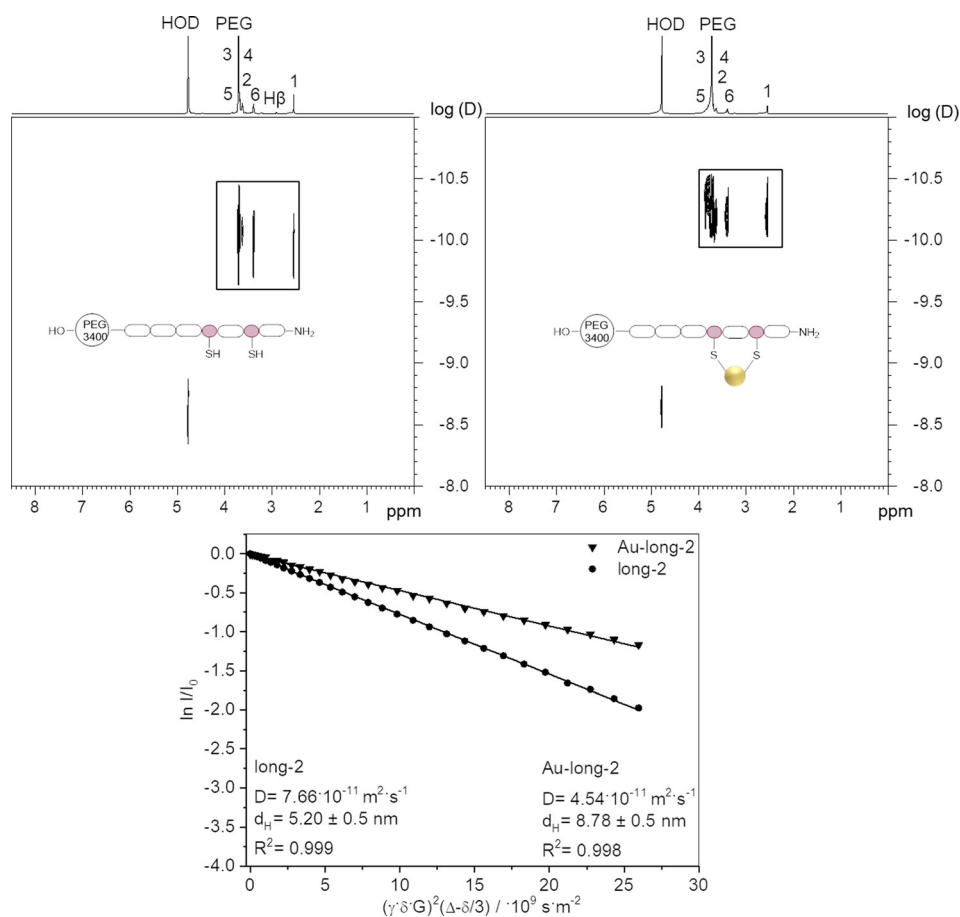
Chemistry–A European Journal

Full Paper
doi.org/10.1002/chem.202003804

Chemistry Europe
European Chemical
Societies Publishing

Figure 5. ^1H DOSY NMR spectrum (500 MHz, 100% D_2O) of the OAA ligand long-2 (top left) and corresponding Stejskal-Tanner plot (bottom). ^1H DOSY NMR spectrum (500 MHz, D_2O) spectrum of Au-long-2 (top right) and corresponding Stejskal–Tanner plot (bottom).
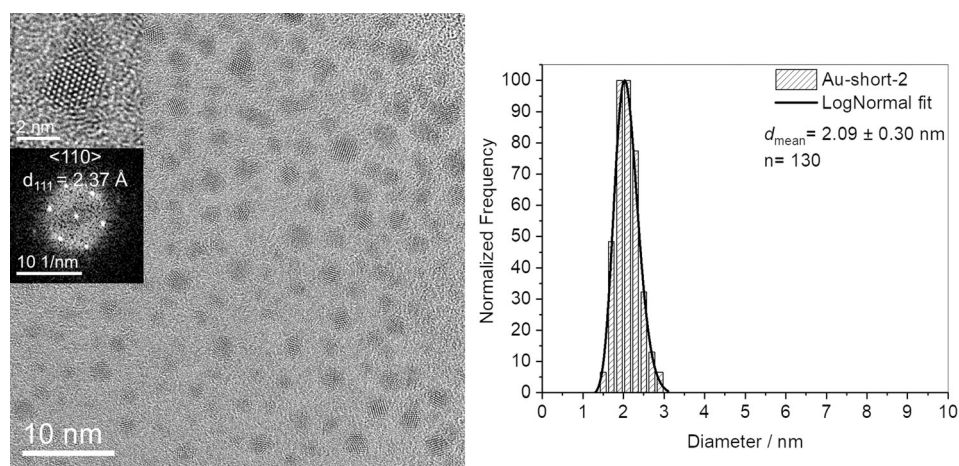

Figure 6. HRTEM image of Au-short-2 gold nanoparticles (left). The manual analysis of 130 particles gave a narrow particle size distribution (right). The organic shell is invisible due to the low contrast, that is, only the gold core is seen.

showed that the hydrodynamic diameter of the particles was significantly larger, that is, 10.33 nm, a fact that can be ascribed to the longer PEG chain of OAA long-6 in comparison to the shorter EDS_3 chain of short-6.

An HRTEM image of Au-long-6 particles is shown in Figure 11. The mean core diameter of the spherical ultrasmall gold nanoparticles was (1.66 ± 0.28) nm. A Fourier transform analysis of the gold core and the analysis of the electron diffraction pattern of the particle gave an interplanar $<111>$ spacing of 2.32 Å, that is, close to the expected value of 2.35 Å.

Chemistry–A European Journal

Full Paper
doi.org/10.1002/chem.202003804

Chemistry Europe
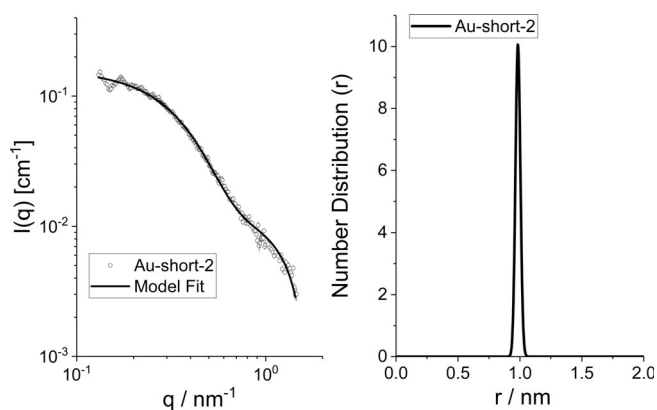European Chemical
Societies Publishing

Figure 7. Small-angle X-ray scattering of dispersed Au-short-2 gold nanoparticles. Left: Primary SAXS data (open symbols) and theoretical model fit (solid line). Right: Size distribution for the nanoparticles.

The results of the SAXS analysis of Au-long-6 nanoparticles are shown in Figure 12. From the model fitting, gold nanoparticles with diameter of (1.7 ± 0.2) nm were obtained with polydispersity of (0.4 ± 0.2) nm. Similarly, as with Au-short-2, a small amount of agglomerates with an average radius of gyration of (4 ± 1) nm (diameter (8 ± 2) nm) were also detected by SAXS analysis.

The degree of functionalization of the nanoparticles was investigated by two different spectroscopic methods: FITC-labeling of the OAAs allowed the quantification by means of a UV/Vis spectroscopic calibration. UV/Vis spectroscopy (Figure 13)

showed OAA ligands bound to ultrasmall gold nanoparticles with the characteristic band of FITC at 495 nm. After a previous calibration with labeled short-2, long-2, short-6, and long-6, respectively, the integration of the FITC absorption band gave the concentration of OAAs in the gold nanoparticle dispersion (using Lambert–Beer's law).

The quantification of the bound OAA ligands to the gold nanoparticles was also achieved by integration of the ^{1}H NMR signals and comparison with an external standard (ERETIC method; *electronic reference to access in vivo concentrations*[22]). The ^{1}H NMR spectra for the quantification of particle-bound OAAs are shown in Figure 14. The signals have a lower resolution than the signals of the previously shown spectra of OAA-functionalized ultrasmall gold nanoparticles. This is due to the absence of water suppression which cannot be applied with the ERETIC method. The pulse of the suppression influences the intensities of the ^{1}H resonances and subsequently affects the integrals of the resonances. The absence of water suppression also causes the broad signal of D_2O in the ^{1}H NMR spectrum which is due to the hydrogen/deuterium exchange.[22]

The ^{1}H NMR spectrum of OAA-functionalized ultrasmall gold nanoparticles in Figure 14 and the external standard were measured with the same pulse program. Peak 2 was used to quantify the bound OAA ligands. This peak belongs to the ^{1}H resonance of the amide α-carbons of the EDS building blocks. These signals were integrated and converted into the concentration of the OAA ligands, taking the proton number into account.
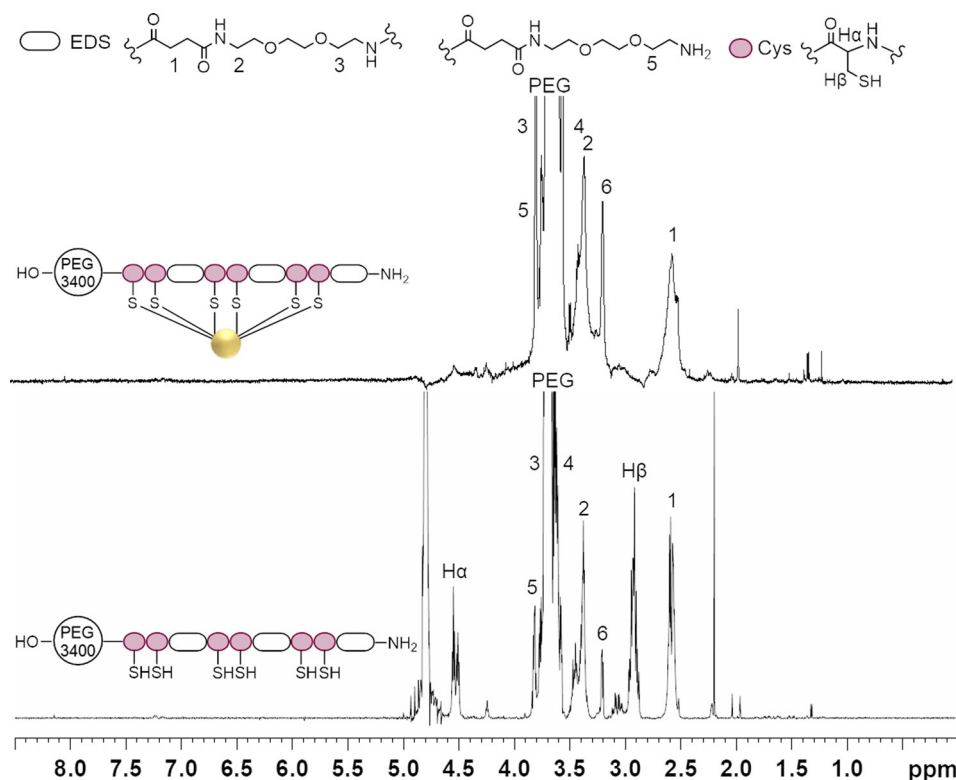

Figure 8. Structure and ^{1}H NMR spectra (600 MHz, 100 % D_2O) of the OAA long-6 (bottom) and of Au-long-6 nanoparticles (top). An ^{1}H NMR spectrum of short-6 is given in the Supplementary Information.
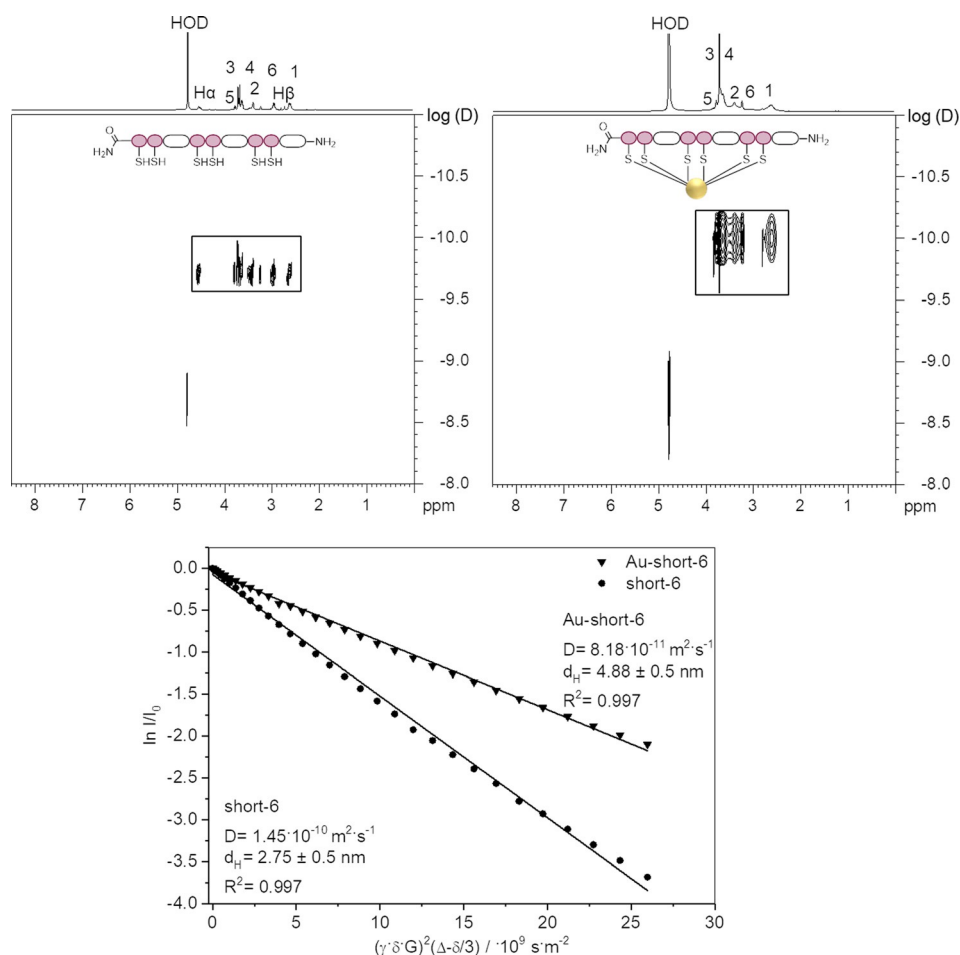
Chemistry–A European Journal

Full Paper
doi.org/10.1002/chem.202003804

Chemistry Europe
European Chemical
Societies Publishing

Figure 9. ^1H DOSY NMR (500 MHz, 100% D_2O) spectrum of dissolved short-6 (top left) and corresponding Stejskal–Tanner plot (bottom). ^1H DOSY NMR (500 MHz, 100% D_2O) spectrum of Au-short-6 nanoparticles (top right) and corresponding Stejskal-Tanner plot (bottom).

Finally, the concentration of the particle-conjugated OAAs was related to the number of gold nanoparticles in the sample. The mass concentration of gold in the samples was determined by AAS. The mass of a nanoparticle was determined using the density of gold and the volume of a nanoparticle with a diameter of 2 nm. The analysis by UV/Vis spectroscopy and by ^1H NMR spectroscopy gave consistent results. However, it must be taken into account that both calculations rely on a number of assumptions (like monodisperse gold particles with spherical shape) that will lead to a considerable error bar. This explains the differences between UV/Vis and ^1H NMR spectroscopy which were obtained from the same samples.

Table 1 summarizes all structural and compositional data.

As expected, there were only small differences within the systems short-2/short-6 and long-2/long-6 when considering the dissolved macromolecules. The PEG chain in the "long"-systems clearly increased the hydrodynamic diameter. This was also found for the gold-conjugated nanoparticles where the systems Au-short-2/Au-short-6 and Au-long-2/Au-long-6 had very similar properties, respectively. However, the systems with 6 cysteine units, that is, Au-short-6/Au-long-6 appeared to

have slightly larger hydrodynamic diameters than the corresponding systems Au-short-2/Au-long-2.

The footprints of the ligands on the gold nanoparticles show that the number of ligands per nanoparticles is different for ligands containing 2 cysteine units (short-2 and long-2) and ligands containing 6 cysteine units (short-6 and long-6). As expected, the number of bound macromolecules decreases with an increasing number of thiol groups within a macromolecule, confirming the expectation that the backbone of the macromolecules lies on the nanoparticle surface. Each cysteine group occupies about 0.074 nm^2. In principle (i.e. numerically), a stable surface functionalization of an ultrasmall gold nanoparticle with 2 nm diameter and a surface area of 12.6 nm^2 could be realized by one OAA carrying about 170 cysteine units. Interestingly, the addition of the PEG group did not have a significant effect on the number of ligands per nanoparticle, thus further highlighting the importance of the OAA segment to control the nanoparticle functionalization. The footprint of a cysteine molecule on 1.8 nm $Au_{ca.174}(cysteine)_{ca.67}$ nanoparticles was about 0.15 nm^2.[5b] This is about two times the value of OAAs, indicating a denser packing of the OAAs on the nanoparticle surface, possibly induced by non-covalent interactions between the ligands.
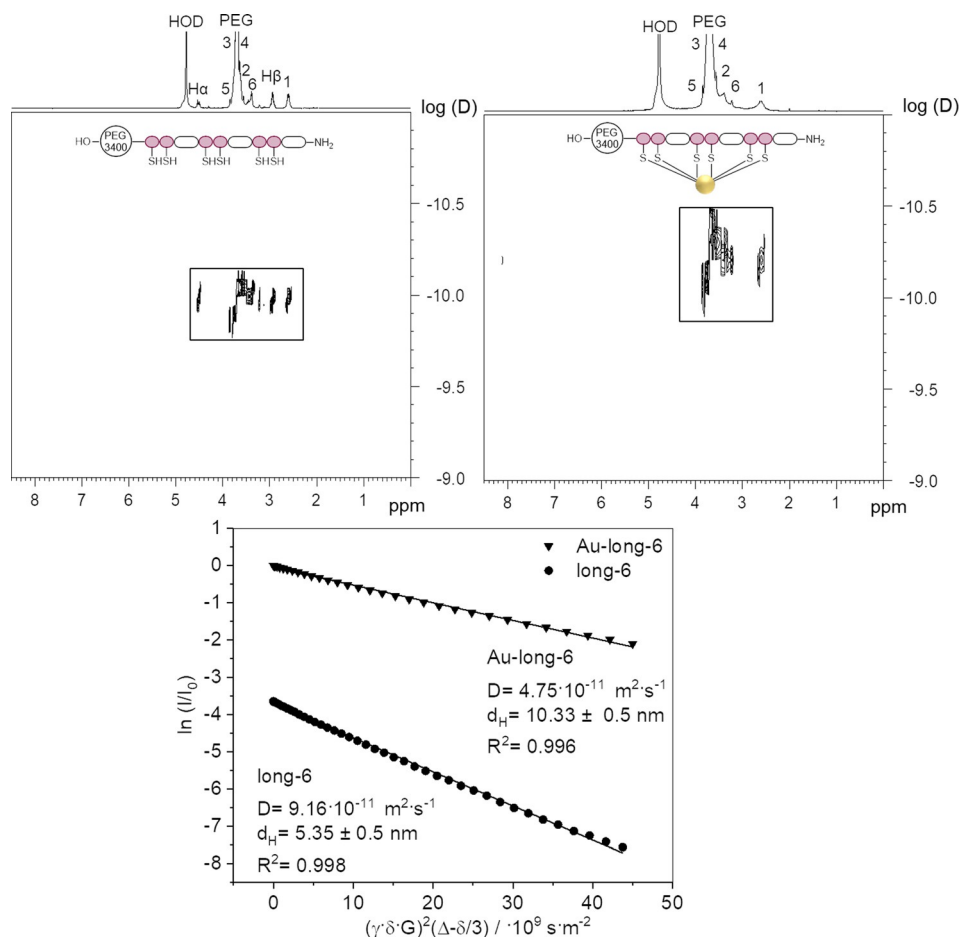
Chemistry–A European Journal

Full Paper
doi.org/10.1002/chem.202003804

Chemistry Europe
European Chemical
Societies Publishing

Figure 10. ^1H DOSY NMR (500 MHz, 100% D_2O) spectrum of dissolved long-6 (top left) and corresponding Stejskal–Tanner plot (bottom). ^1H DOSY NMR (500 MHz, 100% D_2O) spectrum of Au-long-6 nanoparticles (top right) and corresponding Stejskal–Tanner plot (bottom).
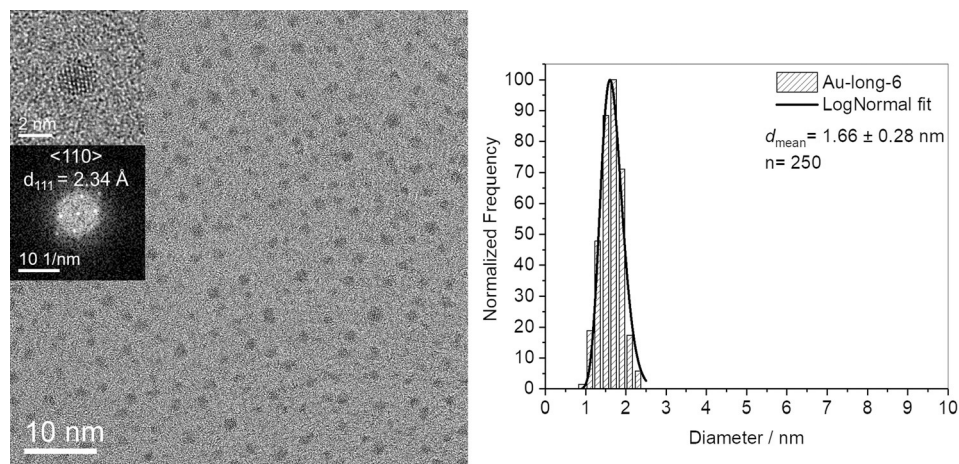

Figure 11. HRTEM image of Au-long-6 nanoparticles (left). The manual analysis of 250 particles gave a narrow particle size distribution (right). The organic shell was invisible due to the low contrast.

It is well understood for polymers attached to gold nanoparticles[23] crystallizing in the face-centered cubic (fcc) structure[24] that the degree of functionalization is affected by the hydrodynamic size of the polymer. Density functional theory (DFT) calculations have shown that Au-S bonding arises from the hybridization of p-like S orbitals with d-like Au orbitals.[25] Ultrasmall nanoparticles with fcc structure can show different shapes like tetrahedra, cuboctahedra, or truncated octahedra.[5b,26] DFT calculations have also shown that the adsorption energy of sulfur on the surface of different fcc metals like Au,
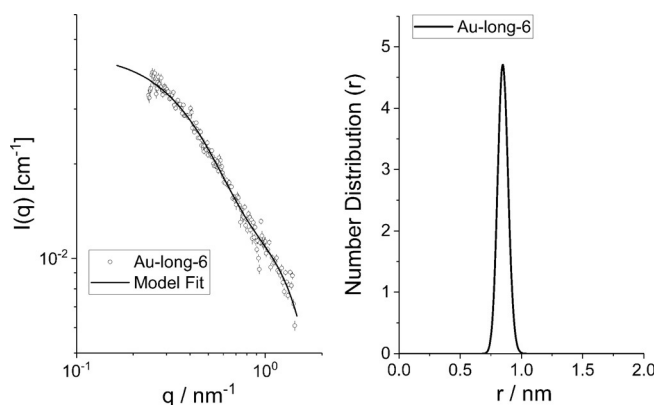
Chemistry–A European Journal

Full Paper
doi.org/10.1002/chem.202003804

Chemistry Europe
European Chemical
Societies Publishing

Figure 12. Small-angle X-ray scattering of Au-long-6 nanoparticles. Left: SAXS data (open symbols) and theoretical model fit (solid line). Right: Size distribution for the ultrasmall gold nanoparticles.

Ag, Cu and Pt follows the general trend (100) ≈ (110) > (111).[27] In addition to the strong covalent and ionic metal-sulfur bonds, van der Waals dispersive forces provide further possibilities which is especially interesting for S-carrying ligands by bringing more atoms of a ligand molecule to the gold surface.[26a] In general, attractive or repulsive forces, for example, based on van der Waals forces, hydrogen bonding, or electrostatic interactions between the ligands influence the number of molecules that can be accommodated on the gold nanoparticle surface. For example, Lanterna et al. have demonstrated that with increasing length of alkyl chains and thus a denser packing based on stronger van der Waals interactions,

the degree of functionalization can be increased.[28] In our study, noncovalent interactions between the OAA segments as well as the number of thiol groups may affect the ligand density. While we have been careful to design the different OAA segments with a similar length of 12 amino acids and number of amide bonds, each EDS building block accounting for two amino acids, they still differ in their primary sequence and thus potentially in their intra- and intermolecular interaction patterns.

The application of multiple thiol-functionalized ligands for gold nanoparticle functionalization was already demonstrated before but has been mainly used to achieve a higher stability in gold nanoparticle functionalization rather than to tune the degree of functionalization. Nandanan et al. applied a chitosan-like polymer containing six thiol groups.[29] Li et al. used tri-thiol-terminated oligonucleotides for the preparation of DNA–gold nanoparticle conjugates. The tri-thiol head groups of the oligonucleotides led to an improved stability of the nanoparticle conjugates.[30] Kang et al. investigated the relationship between the structure of poly-L-lysine-poly(ethylene glycol) (PLL-PEG) multi-thiolated copolymers and the colloidal stability of gold nanoparticles (15–20 nm) under rather extreme conditions such as high temperatures or in the presence of oxidizing agents. They observed a high thermodynamic stability of the nanoparticle systems when the nanoparticles were functionalized with thiolated PLL-PEG ligands that carried multiple thiol groups and additionally had a steric stabilization by PEG grafts.[31]
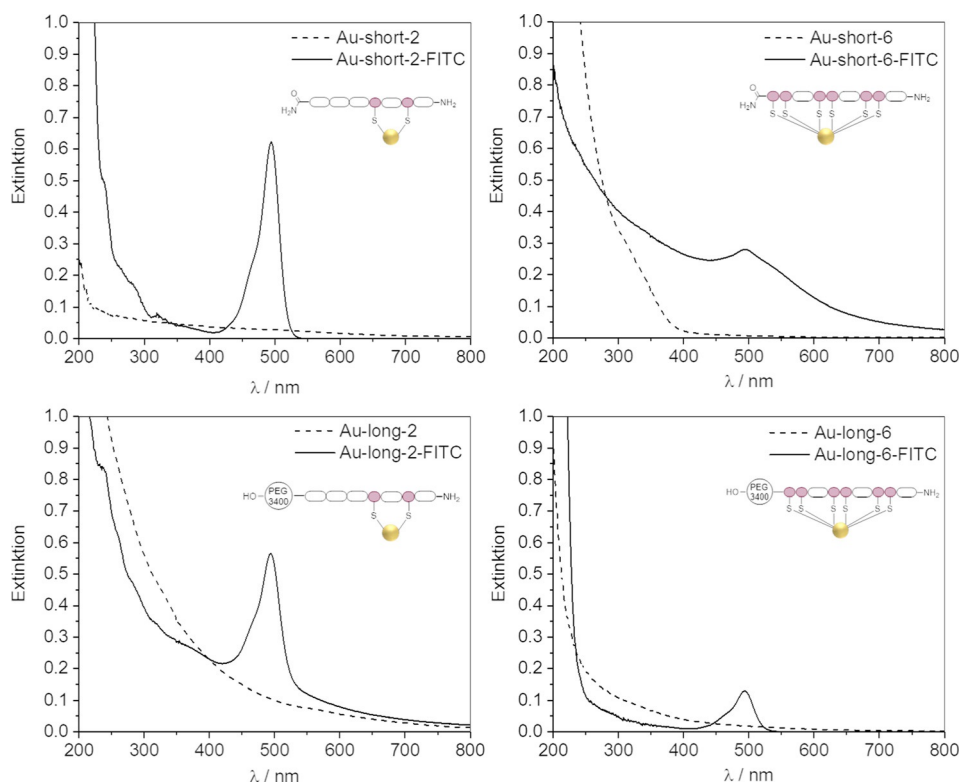

Figure 13. Representative UV/Vis spectra of gold nanoparticles conjugated with different OAAs, both unlabeled and FITC-labeled (solvent: water). The absorption band at 495 nm indicates the fluorescent labeling of long-6 (right) and short-2 (left) for the quantification of conjugated OAAs.
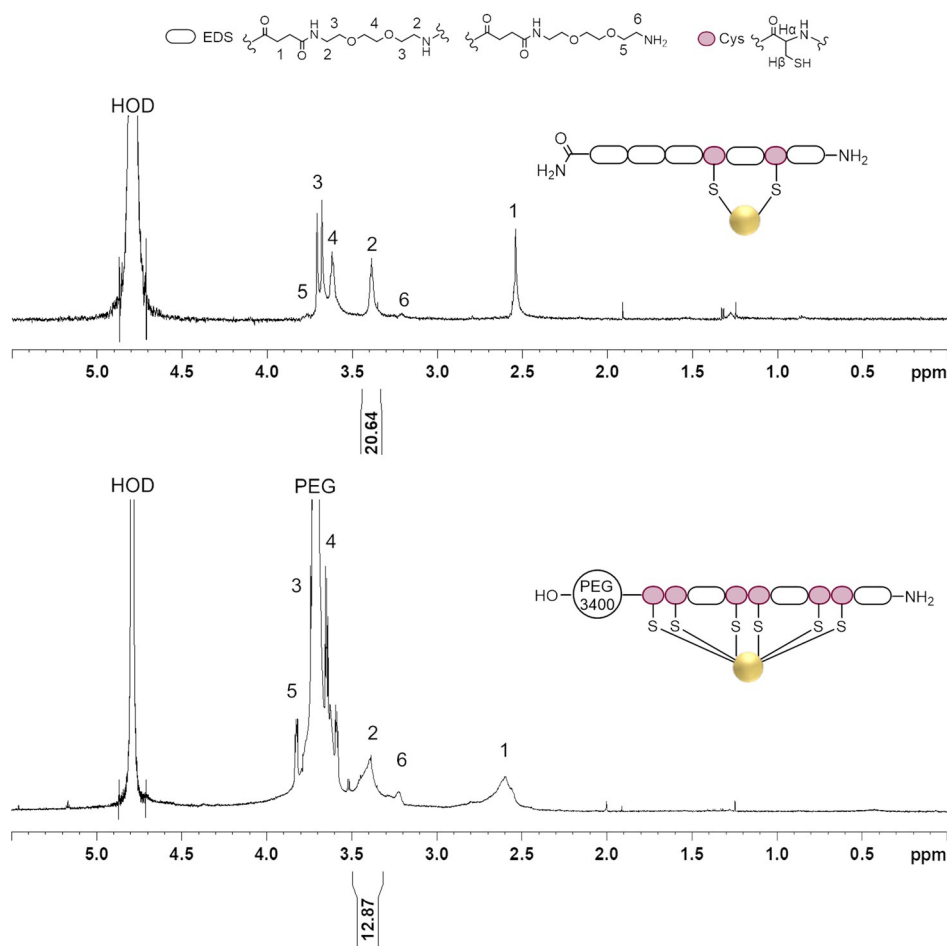
Chemistry–A European Journal

Full Paper
doi.org/10.1002/chem.202003804

Chemistry Europe
European Chemical
Societies Publishing

Figure 14. Representative ^{1}H NMR spectrum (600 MHz, 100% D_2O) of Au-short-2 nanoparticles (top) and of Au-long-6 nanoparticles (bottom) for the quantification of bound OAAs by ERETIC.

Free ligand or Particle	Diameter gold core HRTEM/nm	Hydrodynamic diameter ^{1}H DOSY/nm	Diameter gold core SAXS/nm	Ligands per gold nanoparticle NMR (ERETIC)	Ligands per gold nanoparticle UV/Vis	Footprint per ligand/ nm^2	Footprint per ligand per cysteine/nm^2
short-2	–	2.2 ± 0.5	–	–	–	–	–
Au-short-2	2.1 ± 0.3	3.8 ± 0.5	2.0 ± 0.2	53 ± 11	66 ± 13	0.21 ± 0.04	0.10 ± 0.02
long-2	–	5.2 ± 0.5	–	–	–	–	–
Au-long-2	–	8.8 ± 0.5	–	69 ± 14	99 ± 20	0.15 ± 0.03	0.075 ± 0.015
short-6	–	2.8 ± 0.5	–	–	–	–	–
Au-short-6	–	4.9 ± 0.5	–	37 ± 8	39 ± 8	0.33 ± 0.06	0.055 ± 0.01
long-6	–	5.4 ± 0.5	–	–	–	–	–
Au-long-6	1.7 ± 0.3	10.3 ± 0.5	1.7 ± 0.2	28 ± 6	36 ± 7	0.40 ± 0.08	0.067 ± 0.011

Table 1. Particle size and ligand quantification data for all OAA-conjugated ultrasmall gold nanoparticles.[a]

[a] HRTEM and SAXS give the diameter of the metallic gold core, and ^{1}H DOSY gives the hydrodynamic diameter of water-dispersed nanoparticles. All results indicate a stable gold core during the surface functionalization. The errors in the ligand numbers per nanoparticle are estimated to $\pm 20\%$. All calculations are based on an average diameter of the metallic core of the gold nanoparticles of 2 nm (surface area 12.6 nm^2). The footprint per ligand was computed as average from the NMR spectroscopy and UV results.

In this study, we have explored multiple thiol-functionalized ligands as an alternative strategy to tune the degree of functionalization of gold nanoparticles. Instead of using a single terminal thiol group for anchoring onto the gold nanoparticle surface, we have used specifically designed OAAs presenting multiple thiols. Thereby, a large area of the gold nanoparticle surface should be covered by each OAA molecule, allowing us to vary the number of ligands per particle by varying the number of thiol motifs of each OAA. Indeed, we have found that increasing the number of thiol groups from two to six, the number of surface bound ligands decreased by factors of 1.4 to 2.4 (comparing the short and the long ligands, see

Table 1). This indicates that the correlation between the number of thiol groups in the OAA segment and the degree of functionalization do not correlate linearly, although additional experiments are required to examine this further.

We hypothesize that not only the number of thiol groups affects the surface loading, but also non-covalent interactions between the ligands. While we have seen no evidence of crosslinking of particles via the multiple thiol-containing ligands, going to OAAs with even more than six thiol groups might be challenging in terms of intra- and intermolecular crosslinking. Thus, in order to achieve even lower degrees of functionalization with the final goal of potentially attaching a single ligand onto an ultrasmall gold nanoparticle, the OAA structures will be further developed for example, by going to branched structures and introducing charged moieties.

Conclusions

Precision macromolecules were designed as multivalent ligands to coat the surface of ultrasmall gold nanoparticles. Their surface binding requirements as indicated by the ligand footprint depend on the number of integrated cysteine units (here: either two or six). In general, each cysteine unit occupies about 0.075 nm^2 on the gold nanoparticle surface which is about half of the value of individual cysteine molecules. This indicates an increasing degree of crowding on the particle surface with the ligand, possibly promoted by non-covalent interactions of the ligand molecules. The ligand-conjugated gold nanoparticles were colloidally stable and well dispersed in water. Any cross-conjugation between nanoparticles induced by the multivalent ligands was minor as indicated by small-angle X-ray scattering. The attachment of a PEG chain to the macromolecular ligands considerably increased the hydrodynamic diameter of the dissolved macromolecules and the macromolecule-conjugated gold nanoparticles. Overall, by adapting the number of thiol groups within the precision macromolecule ligand, different degrees of functionalization could be realized and now give access to a library of ligand-functionalized ultrasmall gold nanoparticles.

Acknowledgements

Conflict of interest

The authors declare no conflict of interest.

[1] R. B. Merrifield, *J. Am. Chem. Soc.* **1963**, *85*, 2149–2154.

[2] a) D. Ponader, F. Wojcik, F. Beceren-Braun, J. Dernedde, L. Hartmann, *Biomacromolecules* **2012**, *13*, 1845–1852; b) S. A. Hill, C. Gerke, L. Hartmann, *Chem. Asian J.* **2018**, *13*, 3611–3622.

[3] a) S. Boden, F. Reise, J. Kania, T. K. Lindhorst, L. Hartmann, *Macromol. Biosci.* **2019**, *19*, 1800425; b) K. S. Bücher, P. B. Konietzny, N. L. Snyder, L. Hartmann, *Chem. Eur. J.* **2019**, *25*, 3301–3309; c) F. Shamout, A. Monaco, G. Yilmaz, C. R. Becer, L. Hartmann, *Macromol. Rapid Commun.* **2020**, *41*, 1900459.

[4] S. Boden, K. G. Wagner, M. Karg, L. Hartmann, *Polymers* **2017**, *9*, 716.

[5] a) B. Schuetze, C. Mayer, K. Loza, M. Gocyla, M. Heggen, M. Epple, *J. Mater. Chem. B* **2016**, *4*, 2179–2189; b) T. Ruks, C. Beuck, T. Schaller, F. Niemeyer, M. Zähres, K. Loza, M. Heggen, U. Hagemann, C. Mayer, P. Bayer, M. Epple, *Langmuir* **2019**, *35*, 767–778; c) S. B. van der Meer, K. Loza, K. Wey, M. Heggen, C. Beuck, P. Bayer, M. Epple, *Langmuir* **2019**, *35*, 7191–7204; d) V. Sokolova, G. Nzou, S. B. van der Meer, T. Ruks, M. Heggen, K. Loza, N. Hagemann, F. Murke, B. Giebel, D. M. Hermann, A. J. Atala, M. Epple, *Acta Biomater.* **2020**, *111*, 349–362; e) C. J. Zeng, *Pure Appl. Chem.* **2018**, *90*, 1409–1427; f) L. Xiong, S. Yang, X. X. Sun, J. S. Chai, B. Rao, L. H. Yi, M. Z. Zhu, Y. Pei, *J. Phys. Chem. C* **2018**, *122*, 14898–14907; g) N. A. Sakthivel, A. Dass, *Acc. Chem. Res.* **2018**, *51*, 1774–1783; h) S. Kenzler, C. Schrenk, A. R. Frojd, H. Hakkinen, A. Z. Clayborne, A. Schnepf, *Chem. Commun.* **2018**, *54*, 248–251; i) G. Salassa, A. Sels, F. Mancin, T. Burgi, *ACS Nano* **2017**, *11*, 12609–12614; j) M. Azubel, A. L. Koh, K. Koyasu, T. Tsukuda, R. D. Kornberg, *ACS Nano* **2017**, *11*, 11866–11871; k) T. Mori, T. Hegmann, *J. Nanoparticle Res.* **2016**, *18*, 295; l) M. Azubel, R. D. Kornberg, *Nano Lett.* **2016**, *16*, 3348–3351; m) Y. Chen, C. Zeng, C. Liu, K. Kirschbaum, C. Gayathri, R. R. Gil, N. L. Rosi, R. Jin, *J. Am. Chem. Soc.* **2015**, *137*, 10076–10079; n) M. Cui, Y. Zhao, Q. Song, *TrAC Trends Anal. Chem.* **2014**, *57*, 73–82; o) M. Azubel, J. Koivisto, S. Malola, D. Bushnell, G. L. Hura, A. L. Koh, H. Tsunoyama, T. Tsukuda, M. Pettersson, H. Hakkinen, R. D. Kornberg, *Science* **2014**, *345*, 909–912; p) K. Salorinne, T. Lahtinen, J. Koivisto, E. Kalenius, M. Nissinen, M. Pettersson, H. Häkkinen, *Anal. Chem.* **2013**, *85*, 3489–3492; q) Y. Lu, W. Chen, *Chem. Soc. Rev.* **2012**, *41*, 3594–3623; r) H. Schnöckel, A. Schnepf, R. L. Whetten, C. Schenk, P. Henke, *Z. Anorg. Allg. Chem.* **2011**, *637*, 15–23; s) J. F. Parker, C. A. Fields-Zinna, R. W. Murray, *Acc. Chem. Res.* **2010**, *43*, 1289–1296; t) H. Häkkinen, M. Walter, H. Grönbeck, *J. Phys. Chem. B* **2006**, *110*, 9927–9931; u) Y. Negishi, K. Nobusada, T. Tsukuda, *J. Am. Chem. Soc.* **2005**, *127*, 5261–5270; v) G. Schmid, R. Pfeil, R. Boese, F. Bandermann, S. Meyer, G. H. M. Calis, J. W. A. van der Velden, *Chem. Ber.* **1981**, *114*, 3634–3642; w) M. Fischler, A. Sologubenko, J. Mayer, G. Clever, G. Burley, J. Gierlich, T. Carell, U. Simon, *Chem. Commun.* **2008**, 169–171.

[6] J. Turkevich, P. C. Stevenson, J. Hilliery, *Discuss. Faraday Soc.* **1951**, *11*, 55.

[7] a) Y. C. Yeh, B. Creran, V. M. Rotello, *Nanoscale* **2012**, *4*, 1871–1880; b) K. Saha, S. S. Agasti, C. Kim, X. Li, V. M. Rotello, *Chem. Rev.* **2012**, *112*, 2739–2779; c) W. J. Stark, *Angew. Chem. Int. Ed.* **2011**, *50*, 1242–1258; *Angew. Chem.* **2011**, *123*, 1276–1293; d) R. Sardar, A. M. Funston, P. Mulvaney, R. W. Murray, *Langmuir* **2009**, *25*, 13840–13851; e) R. A. Sperling, P. Rivera, F. Zhang, M. Zanella, W. J. Parak, *Chem. Soc. Rev.* **2008**, *37*, 1896–1908; f) K. Zarschler, L. Rocks, N. Licciardello, L. Boselli, E. Polo, K. P. Garcia, L. De Cola, H. Stephan, K. A. Dawson, *Nanomedicine* **2016**, *12*, 1663–1701.

Chemistry–A European Journal

Full Paper
doi.org/10.1002/chem.202003804

Chemistry Europe
European Chemical
Societies Publishing

[8] a) G. Salassa, T. Burgi, *Nanoscale Horiz.* **2018**, *3*, 457; b) C. Guo, J. L. Yarger, *Magn. Reson. Chem.* **2018**, *56*, 1074–1082; c) A. M. Smith, L. E. Marbella, K. A. Johnston, M. J. Hartmann, S. E. Crawford, L. M. Kozycz, D. S. Seferos, J. E. Millstone, *Anal. Chem.* **2015**, *87*, 2771–2778; d) S. Aryal, B. K. C. Remant, N. Dharmaraj, N. Bhattarai, C. H. Kim, H. Y. Kim, *Spectrochim. Acta A.* **2006**, *63*, 160–163.

[9] M. Baier, M. Giesler, L. Hartmann, *Chem. Eur. J.* **2018**, *24*, 1619–1630.

[10] M. F. Ebbesen, C. Gerke, P. Hartwig, L. Hartmann, *Polym. Chem.* **2016**, *7*, 7086–7093.

[11] M. Brust, J. Fink, D. Bethell, D. J. Schiffrin, C. Kiely, *Chem. Commun.* **1995**, 1655–1656.

[12] A. Thust, J. Barthel, K. Tillmann, *J. Large-Scale Res. Fac.* **2016**, *2*, A41.

[13] a) A. S. Altieri, D. P. Hinton, R. A. Byrd, *J. Am. Chem. Soc.* **1995**, *117*, 7566–7567; b) E. O. Stejskal, J. E. Tanner, *J. Chem. Phys.* **1965**, *42*, 288.

[14] G. Kellermann, F. Vicentin, E. Tamura, M. Rocha, H. Tolentino, A. Barbosa, A. Craievich, I. Torriani, *J. Appl. Crystallogr.* **1997**, *30*, 880–883.

[15] L. P. Cavalcanti, I. L. Torriani, T. S. Plivelic, C. L. P. Oliveira, G. Kellermann, R. Neuenschwander, *Rev. Sci. Instrum.* **2004**, *75*, 4541–4546.

[16] A. P. Hammersley, S. O. Svensson, M. Hanfland, A. N. Fitch, D. Hausermann, *Adv. High Pressure Res.* **1996**, *14*, 235–248.

[17] P. R. A. F. Garcia, K. Loza, S. Daumann, V. Grasmik, K. Pappert, A. Rostek, J. Helmlinger, O. Prymak, M. Heggen, M. Epple, C. L. P. Oliveira, *Braz. J. Phys.* **2019**, *49*, 183–190.

[18] K. Rahme, L. Chen, R. G. Hobbs, M. A. Morris, C. O'Driscoll, J. D. Holmes, *RSC Adv.* **2013**, *3*, 6085–6094.

[19] I. Hussain, S. Graham, Z. Wang, B. Tan, C. C. Sherrington, S. P. Rannard, A. I. Cooper, M. Brust, *J. Am. Chem. Soc.* **2005**, *127*, 16398–16399.

[20] a) C. L. P. Oliveira, in *Current Trends in X-ray Crystallography* (Ed.: D. A. Chandrasekaran), InTech, **2011**, pp. 367–392; b) P. R. A. F. Garcia, O. Prymak, V. Grasmik, K. Pappert, W. Wlysses, L. Otubo, M. Epple, C. L. P. Oliveira, *Nanoscale Adv.* **2020**, *2*, 225–238.

[21] D. Mahl, J. Diendorf, W. Meyer-Zaika, M. Epple, *Coll. Surf. A* **2011**, *377*, 386–392.

[22] S. Akoka, L. Barantin, M. Trierweiler, *Anal. Chem.* **1999**, *71*, 2554–2557.

[23] Y. Que, C. Feng, S. Zhang, X. Huang, *J. Phys. Chem. C* **2015**, *119*, 1960–1970.

[24] M. Song, G. Zhou, N. Lu, J. Lee, E. Nakouzi, H. Wang, D. Li, *Science* **2020**, *367*, 40–45.

[25] a) F. P. Cometto, P. Paredes-Olivera, V. A. Macagno, E. M. Patrito, *J. Phys. Chem. B* **2005**, *109*, 21737–21748; b) J. Gottschalck, B. Hammer, *J. Chem. Phys.* **2002**, *116*, 784–790; c) R. Di Felice, A. Selloni, E. Molinari, *J. Phys. Chem. B* **2003**, *107*, 1151–1156.

[26] a) M. García-Diéguez, D. D. Hibbitts, E. Iglesia, *J. Phys. Chem. C* **2019**, *123*, 8447–8462; b) M.-C. Saint-Lager, I. Laoufi, A. Bailly, O. Robach, S. Garaudée, P. Dolle, *Faraday Discuss.* **2011**, *152*, 253–265; c) V. Tripković, I. Cerri, T. Bligaard, J. Rossmeisl, *Catal. Lett.* **2014**, *144*, 380–388; d) S. Banerjee, C. H. Liu, J. D. Lee, A. Kovyakh, V. Grasmik, O. Prymak, C. Koenigsmann, H. Liu, L. Wang, A. M. M. Abeykoon, S. S. Wong, M. Epple, C. B. Murray, S. J. L. Billinge, *J. Phys. Chem. C* **2018**, *122*, 29498–29506.

[27] C. R. B. Rodríguez, J. A. Santana, *J. Chem. Phys.* **2018**, *149*, 204701.

[28] A. E. Lanterna, E. A. Coronado, A. M. Granados, *J. Phys. Chem. C* **2012**, *116*, 6520–6529.

[29] E. Nandanan, N. R. Jana, J. Y. Ying, *Adv. Mater.* **2008**, *20*, 2068–2073.

[30] Z. Li, R. Jin, C. A. Mirkin, R. L. Letsinger, *Nucleic Acids Res.* **2002**, *30*, 1558–1562.

[31] J. S. Kang, T. A. Taton, *Langmuir* **2012**, *28*, 16751–16760.